coatings

MDPI

Article

Laser-Assisted Surface Texturing of Ti/Zr Multilayers for Mesenchymal Stem Cell Response

Suzana Petrović [1,*], Davor Peruško [1], Evangelos Skoulas [2], Janez Kovač [3], Miodrag Mitrić [1], Jelena Potočnik [1], Zlatko Rakočević [1] and Emmanuel Stratakis [2]

1 Vinča Institute of Nuclear Sciences, University of Belgrade, P.O. Box 522, 11001 Belgrade, Serbia; dperusko@vin.bg.ac.rs (D.P.); mmitric@vin.bg.ac.rs (M.M.); jpotocnik@vin.bg.ac.rs (J.P.); zlatkora@vin.bg.ac.rs (Z.R.)

2 Institute of Electronic Structure and Laser (IESL), Foundation for Research and Technology (FORTH), N. Plastira 100, Vassilika Vouton, 70013 Heraklion, Crete, Greece; skoulasv@iesl.forth.gr (E.S.); stratak@iesl.forth.gr (E.S.)

3 Jožef Stefan Institute, Jamova 39, 1000 Ljubljana, Slovenia; Janez.kovac@ijs.si

* Correspondence: spetro@vin.bg.ac.rs; Tel.: +381-11-3408560

Received: 6 November 2019; Accepted: 10 December 2019; Published: 13 December 2019

Abstract: The formation of an ordered surface texture with micro and nanometer features on Ti/Zr multilayers is studied for better understanding and improvement of cell integration. Nanocomposite in form 30×(Ti/Zr)/Si thin films was deposited by ion sputtering on Si substrate for biocompatibility investigation. Surface texturing by femtosecond laser processing made it possible to form the laser-induced periodic surface structure (LIPSS) in each laser-written line. At fluence slightly above the ablation threshold, beside the formation of low spatial frequency-LIPSS (LSFL) oriented perpendicular to the direction of the laser polarization, the laser-induced surface oxidation was achieved on the irradiated area. Intermixing between the Ti and Zr layers with the formation of alloy in the sub-surface region was attained during the laser processing. The surface of the Ti/Zr multilayer system with changed composition and topography was used to observe the effect of topography on the survival, adhesion and proliferation of the murine mesenchymal stem cells (MSCs). Confocal and SEM microscopy images showed that cell adhesion and their growth improve on these modified surfaces, with tendency of the cell orientation along of LIPSS in laser-written lines.

Keywords: multilayer thin films; Ti-based alloy; ultrafast laser-modification; cell response

1. Introduction

Thin films and coatings are considered as very applicable for biomaterials, since surface properties are a key factor in the interaction of materials with the biological environment. Surface composition and morphology regulate surface bioactivity and other biofunctionalities, in terms of the adsorption of proteins on the material surface, which is determinant for the subsequent processes of cell growth, differentiation, and extracellular matrix formation [1–3]. Titanium-based materials are nowadays well integrated into the body, due to high specific strength, excellent corrosion resistance, and good biocompatibility [4,5]. Currently, one of the main tasks is development of the Ti-based alloys with a high concentration of β-stabilizer elements (β phase of titanium), and to provide compliance between the elasticity of the implant and the surrounding hard tissues (bones). The most suitable alloying elements to be added in these new alloys are niobium, tantalum, zirconium, and molybdenum, as they do not exhibit any cytotoxic reaction in contact with cells [6]. The admissible way for preparation of Ti-based alloy coatings could be deposition of multilayer structure with alternate distribution of Ti and other (Zr, Ta, Mo, Nb) components in thin films. The superior biocompatibility of Ti-based coatings

originates in easy formation of outer Ti-oxide layer with a negative charge at physiological pH and protects against the metallic components dissolving in biological fluids [7]. One promising candidate for alloying is Zr, which act as a neutral element when dissolved in Ti and can improve mechanical properties of alloys [7]. From the biomedical point of view, Zr is fully soluble in both allotropic phases of Ti, improving the mechanical strength, corrosion resistance, and biocompatibility of Ti alloys [8]. Zirconium (Zr) has received special attention as an alloying element in Ti-based alloys, because it acts like non-toxic and non-allergenic elements, thereby avoiding stress shielding effects and implant failure [9]. Binary Ti–Zr alloy has exhibited a good combination of mechanical properties, with the advantage of easy manufacturing, in comparison to multicomponent, Ti-based alloys. Additionally, Zr with the lower elastic modulus (~80 GPa) can contribute to reducing stress shielding, which is the reason for the biomechanical incompatibility between the pure Ti-based implant and the bone [10].

Currently, more sophisticated and versatile methods/tools for surface engineering and synthesis of nanoscale facilities for biomedical applications are needed. In traditional chemical and physical methods, although the microstructure can be controlled to some extent, the specific shape and size in some particular applications cannot be precisely controlled. Most of the traditional methods have disadvantages, such as low efficiency, high cost and difficult-to-machine. By contrast, laser processing can easily form and control desired complicated topography with high resolution and high economic efficiency [11,12]. Techniques based on laser surface modification have advantages such as less debris contamination, reproducibility, precision and minimal heat-affected zone, which can create a controlled surface texture in specific, localized areas in a short time period [13]. Femtosecond laser texturing is a mask-free contactless technology, fully adaptable for 2D and 3D shapes on almost all materials [14]. The surface modification of the biomaterial has aimed to create specific chemical and physical properties that offer a favorable cellular response [15,16]. On the other hand, ultrafast laser surface modification is a unique method, which allows production of bioactive surface with formation of the desired oxide and alloy, creation of nano/micro textures and change wettability of the surface. Surface topographies with defined micro- and nanometer features generated by irradiation with linearly polarized laser radiation are well known as a laser-induced periodic surface structure (LIPSS). These surface structures have appeared in two forms as low spatial frequency LIPSS (LSFL) and high spatial frequency LIPSS (HSFL) [17]. The LSFLs usually have a spatial period close to the irradiation wavelength, oriented perpendicularly to the polarization vector. LSFL is generally accepted to originate from the interaction of the incident laser beam and electromagnetic wave scattered at the surface with the possibility to involve the excitation surface plasmon polariton. On the other hand, the HSFLs, oriented parallel to the polarization vector, are characterized with significantly lower periodicity than the irradiation wavelength. Several physical mechanisms have been proposed to explain the formation of HSFLs induced by laser pulses, such as self-organization, second harmonic generation, excitation of surface plasmon polaritons, and Coulomb explosion, but none have been proven fully yet [18]. The initial interactions between osteoblasts and nano-modified polymeric, ceramic and metallic substrates have indicated that nanoscale roughness can significantly affect cell adhesion, proliferation, and spreading. A few studies have indicated that increased osteoblast proliferation on the nanostructured surfaces coincided with an increase in alkaline-phosphatase synthesis, increased Ca-containing mineral deposition, and higher immunostaining of osteocalcin and osteopontin [19]. Recently, it has been demonstrated that osteointegration can be accelerated if the titanium surface is pre-treated to have a specific topography containing both micro- and nano-scale features [13]. In vivo experiments have shown that titanium and zirconium implants exhibit good osteointegration and that both elements have a high degree of bone-implant contact [20,21].

The aim of this paper is to study the relationship between laser processing and osteoblast-like cell response on titanium–zirconium multilayer thin films. The formation of an ordered surface line-texture with micro and nanometer features was achieved by optimizing the laser parameters, including applied laser fluences, number of pulses, and scanning rate. The micro/nano patterns distribution with changed composition and surface topography is evaluated in aim to determining their influence

on cell adherence, cell morphology and the possibility of cell orientation along the laser-induced periodic structure.

2. Materials and Methods

The titanium–zirconium multilayer thin films were deposited in a Balzers Sputtron II system, using 1.3 keV argon ions and 99.9% pure Ti and Zr targets. Before deposition, the chamber was evacuated to the base pressure of 1×10^{-6} mbar, while the Ar partial pressure during deposition was 1×10^{-3} mbar. Silicon wafer Si (100) is used as substrate, which was cleaned by etching in HF and immersion in deionized water before mounting in the chamber. The deposition of multilayers was performed in a single vacuum run, at deposition rate of 0.17 nm s^{-1} for both Ti and Zr components, without heating of the substrates. The complete multilayer structure consisted of 30×(Ti/Zr) bilayers with total thickness of 1 μm, where thickness of individual Ti and Zr layers were about 17 nm.

Ultrafast laser modification of the multilayer 30×(Ti/Zr) thin films was performed with the Yb:KGW laser source Pharos SP from Light Conversion. The surface of thin films was irradiated by focused linearly p-polarized pulses with the following characteristics: repetition rate of 1 kHz, pulse duration of 160 fs, central wavelength of 1030 nm and 43 μm Gaussian spot diameter in focus. Samples were laser processed in an open air ambient environment and mounted on a motorized, computer-controlled, X-Y-Z translation stage, at normal incidence to the laser beam. The irradiations were conducted at identical conditions, creating lines on the surface of 5 mm × 5 mm at laser pulse energy of 60 μJ. In each line, energy per pulse was assumed to be constant, since the pulse energy deviation was less than 1%. The irradiation of the samples was performed in defocus mode by positioning the samples out of focus at 4 cm, thereby a pulse fluence of 0.4 J cm^{-2} with a spatial extension of the Gaussian beam profile was achieved. Indirectly, under the given laser irradiation conditions, the width of line with value of 75 μm was adjusted by defocusing of the laser beam, while distances between lines keep constant at value of 80 μm. The lines were direct laser writing at scan velocity of 2 mm s^{-1} (Figure 1).

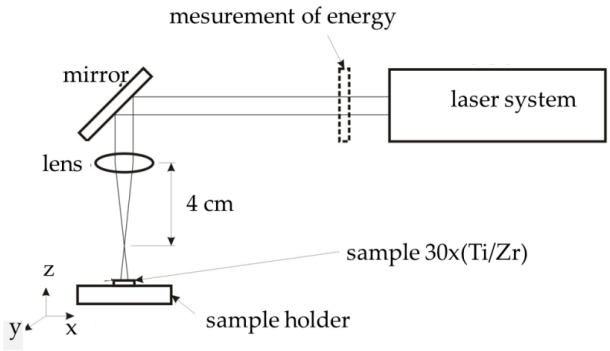

Figure 1. Schema of the experimental setup for laser processing.

Detailed surface morphology after irradiation was examined firstly by optical microscopy, and then by scanning electron microscopy (JEOL JSM-7500F, Tokyo, Japan) equipped with energy-dispersive X-ray spectroscopy (EDS) (High Wycombe, UK). A fracture cross section of the irradiated sample was performed by FEI SCIOS 2 microscopy, Hillsboro, OR, USA. The native cross-section of the sample was simply prepared by made fracture transversely to the laser-written lines. Phase composition and crystal structure analysis with X-ray diffraction (XRD), where the Cu Kα XRD pattern was collected by a Bruker D8 Advance Diffractometer, Karlsruhe, Germany. For these measurements, the Bragg–Brentano geometry with a step of 0.05° and the time interval of 30 s per step was used. The distribution of elements and interfaces of the multilayer 30×(Ti/Zr)/Si system were determined by time-of-flight SIMS instrument (Ion-TOF, Loughborough, UK). For composition depth profiling high energy Ga^+ pulsed primary source (25 keV) was combined with low energy sputter guns at 2 keV (Cs^+ and O^{2+}) at angle of 45° to sample surface.

Cell study under static in vitro conditions was performed with the mouse mesenchymal stem cells (MSCs) line (C57BL/6). MSCs cells were grown in cell culture flasks using Dulbecco's modified Eagle's medium [DMEM (Invitrogen, Grand Island, NY, USA) supplemented with 10% fetal bovine serum (FBS, Biosera, Sussex, UK)] in a 5% CO_2 incubator (Thermo Scientific, Waltham, MA, USA) at 37 °C. Laser-processed samples were autoclaved and transferred into sterile wells of 24 well plates (Sarstedt; Numbrecht, Germany). Culture medium with 2×10^4 cells were seeded onto the samples, where they were cultured in different time periods, ranging from one to three days in order to estimate the cell orientation, adhesion and proliferation. After each time points, the medium with MSCs cells were removed and the cultured samples were washed twice with 0.1 M sodium cacodylate buffer (SCB) and fixed with 2% glutaraldehyde (GDA) and 2% paraformaldehyde (PFA) in 0.1 M SCB for 30 min. Subsequently, samples were washed twice with 0.1 M SCB and dehydrated in increasing concentrations (from 30%–100%) of ethanol. Finally, before the determination of MSCs osteoblast cell morphology, samples were dried in a critical point drier (Baltec CPD 030, London, UK), sputter-coated with thin (10 nm) gold/palladium layer (Baltec SCD 050) and observed by scanning electron microscope (JEOL JSM-6390 LV). The cytoskeleton, focal adhesion points and nucleus of MSCs were stained for actin filaments, vinculin and DAPI. Specifically, after one and three days of cell cultured, the samples were fixed with 4% paraformaldehyde (PFA) for 15 min and permeabilized with 0.1% Triton X-100 in phosphate-buffered saline (PBS) for 5 min. The non-specific binding sites were blocked with 2% bovine serum albumen (BSA) in PBS for 30 min. Cell imaging was performed using a Leica SP8 inverted scanning confocal microscope (Jena, Germany) with ×40 objective.

3. Results and Discussion

The simultaneous creation of micro and nanometer morphological features on the surface of the multilayer Ti/Zr structure for biomedical application was achieved by laser writing of lines with a relatively wide laser beam (75 μm). Morphological shapes in micrometer dimensions consisted of 65 laser-written lines on a surface of 5 mm × 5 mm, whereby the width of each line was approximately 40 μm and the distance between them is also 40 μm (Figure 2a) as a consequence of the Gaussian shape of the laser beam profile. In each laser-written line, the creation of the laser-induced periodic surface structure (LIPSS) occurred, so that they were oriented normally to the direction of laser polarization (Figure 2b,c). These ripple structures are attributed to well-defined low spatial frequency LIPSS (LSFL) as a result of an interference of the incident laser beam with a surface electromagnetic wave excited during the laser irradiation with the possibility to involve the excitation surface plasmon polariton [22,23]. Applying a laser fluence of about 0.4 J cm^{-2}, which is slightly higher than the ablation threshold for the Ti/Zr system (0.22 J cm^{-2}), the LIPSS formation was accompanied by laser ablation of the multilayer 30×(Ti/Zr) thin films, as a consequence of the multi-pulse effect occurring between successive pulses [24]. LSFL ripples were not smooth, indicating the absence of any hydrodynamic effects during laser processing, but rather the dominant direct removal of thin film materials. The fragments were retained after laser ablation at the top of the LSFL ripples, where their appearance could indicate an unequal erosion of the layered structure (Figure 2c). In the zone of laser-written lines, the regular LSFL ripples appeared with a periodicity of approximately 800 nm. At given laser fluence, the ripple length ranges from quite small under 1 μm, to those whose length exceeds 7 μm (Figure 2c). In the cracks between LSFL ripples, the formation of high spatial frequency LIPSS (HSFL) was observed, which could be related to the decrease in energy distributed within the multilayer 30×(Ti/Zr) structure.

On the other hand, the HSFL ripples were formed in the zone between the two laser-written lines as a result of the action and overlapping of the edge Gaussian profile, where the energy is expected to be quite low, below the ablation threshold (Figure 2d,e). These HSFL ripples were oriented perpendicular to LSFL ripples with periodicity close to 200 nm, wherein the width of the individual HSFL ripple was below 100 nm. No ablation of the thin film materials was observed in this zone, so their formation can be attributed to the oxide phase upgrade or inducing the dewetting process [18,25,26].

On that occasion, the absorbed laser energy was induced the surface instabilities due to softening and perturbation of crystal and chemical bindings, as an endorsement of the model of self-organized structure formation. [18]. The solid-state dewetting can be induced during the laser processing as spontaneous regrouping of surface material into small-sized ripples (similar to nanorods) on the hot surface but at temperatures lower than the Ti melting point (Ti is top layer) [27]. Moving away from the laser-written line, the HSFLs gradually disappeared but not completely (Figure 1e), as they became pronounced again from the middle of unmodified area, approaching to the next line.

For the first rough check of the composition changes after laser treatment of 30×(Ti/Zr) system at the pulse fluence of 0.4 J cm^{-2}, the EDS method was used. Despite the used instrument analytical accuracy of $2\sigma = 2\%$, the obtained results should be taken as semi-quantitative because of the small thickness of 30×(Ti/Zr) multilayer system [23,24]. The elemental composition recorded by the EDS method at three different locations, in the center of the laser-written line, at the edge of this line and in the area between the lines, was compared in the spectra presented in Figure 3. Based on the obtained spectra, it can be concluded that there are no drastic changes in the concentrations for Ti, Zr, Si and O components, between the observed areas. It could be distinguished that laser ablation of the Ti/Zr multilayer was registered in the area of the laser-written line, whereby the zirconium was more removed than titanium and concentration of silicon increased in this area. On the other hand, surface oxidation could be observed as an effect of laser processing of the Ti/Zr system, which was reflected in the increasing of the oxygen concentration, especially in the area of the laser-written lines.

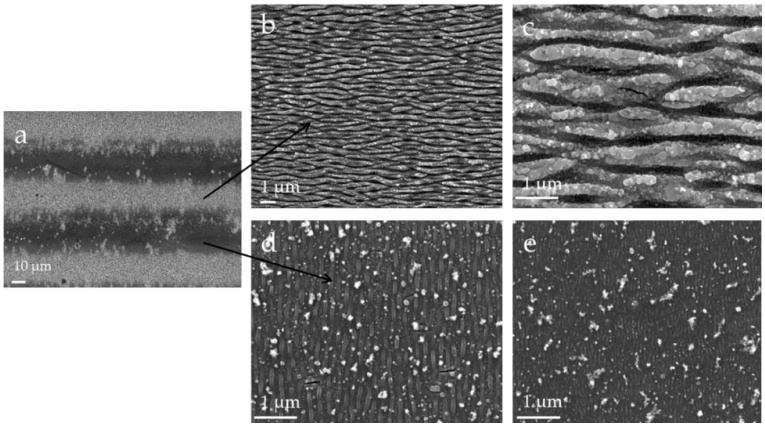

Figure 2. Scanning electron microscope (SEM) microphotographs of the 30×(Ti/Zr)/Si multilayer system after laser processing at laser fluence of 0.4 J cm^{-2}; (**a**) view of laser-written lines at magnification of 500×, (**b**,**c**) view of morphology inside of line with magnification 5000× and 20,000×, respectively and (**d**,**e**) view of morphology between lines at 20,000× magnification.

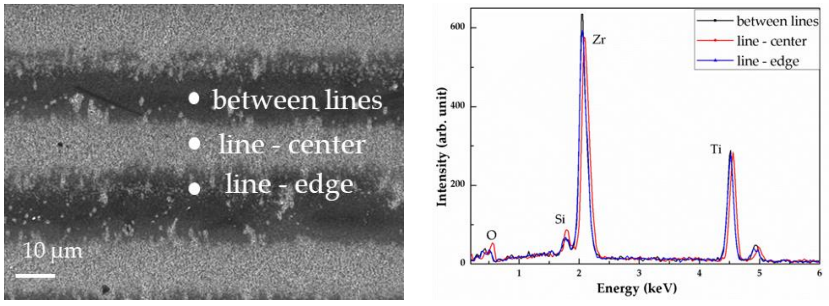

(**a**) (**b**)

Figure 3. SEM microphotographs and energy-dispersive X-ray spectroscopy (EDS) analysis of the 30×(Ti/Zr)/Si multilayer system after laser processing at laser fluence of 0.4 J cm^{-2}; (**a**) view of lase-written lines at magnification of 500× with the positions of the recorded EDS spectra, and (**b**) EDS spectra.

A cross-section view of 30×(Ti/Zr)/Si multilayer system was obtained with SEM microscopy on the broken sample, including the unmodified part and the irradiated area in a place normal to the laser-written lines (Figure 4). Inside the as-deposited 30×(Ti/Zr) multilayer thin film were very well separated and alternately arranged Ti and Zr layers with almost identical thicknesses of individual layers (Figure 4a). The SEM cross-section view of 30×(Ti/Zr)/Si multilayer after laser processing in the zone of the laser-written lines (Figure 4b–d), confirms that the creation of periodical structure in form of LSFL ripples was accompanied by ablation of the material. However, laser ablation was quite unequal by making the number of the removed layers variable and ranged in interval of 8–15 layers (130–250 nm) when viewed at the top of the ripples. The depth of cracks between LSFL ripples were about 20 layers (350 nm), while their repetition period was about 800 nm (Figure 4b), which is consistent with the periodicity of the formed LSFLs. The spatial distribution of Ti and Zr components inside the laser-modified area retained a layered structure, with barely noticeable expansion of the interfaces between the Ti and Zr layers. Also, slight deformation or corrugating of the inner Ti and Zr layers could be observed, most likely by inducing internal stresses during the laser irradiation (Figure 4d).

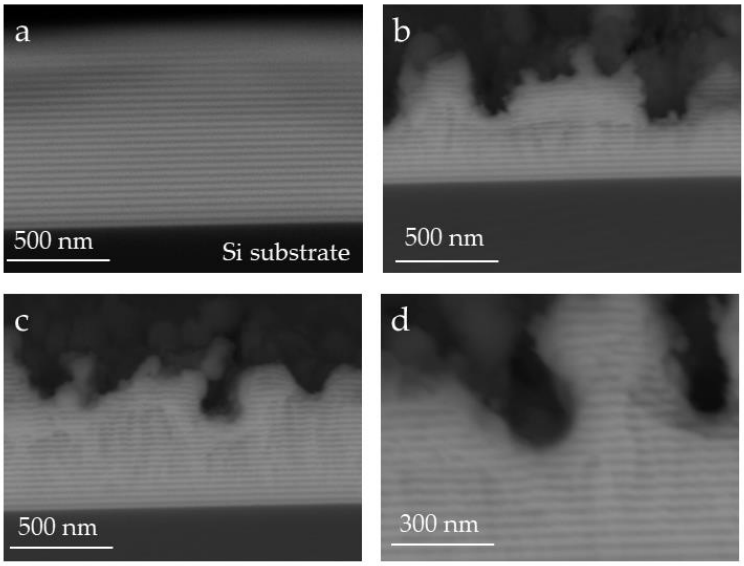

Figure 4. SEM cross-section view of the native broken 30×(Ti/Zr)/Si multilayer sample: (**a**) unmodified part at magnification of 120,000×, (**b**) and (**c**), the irradiated area in a place normal to the laser-written lines at magnification of 120,000×, and (**d**) part of laser-modified sample at 200,000× magnification.

The concentration depth profiles recorded by SIMS technique for the as-deposited and laser processed multilayer 30×(Ti/Zr)/Si system are presented in Figure 5. Results obtained by SIMS analysis of almost half of the as-deposited Ti/Zr multilayer structure showed that the Ti and Zr layers were very well separated with clearly defined interfaces between them (Figure 5a). After femtosecond laser processing of Ti/Zr multilayer structure, the distribution of the components could not be accurately determined, since the roughness of the laser-modified surface was quite high. The differences in height greater than 300 nm were reached, especially at the crack locations between LSFL ripples. In these positions the Si substrate was relatively close to the surface, which can be reason for the appearance of Si component in the spectrum (Figure 5b). In addition, it can be assumed that there was a possible diffusion of Si atoms from the substrate into a thin layer during laser irradiation [25]. The main components Ti and Zr were well intermixed, which is inconsistent with the result obtained by the SEM cross-section analysis, where the layered structure is retained after modification (Figure 5b). These differences can be attributed to the fact that the signal in SIMS analysis was taken from a large sample surface, regardless of the morphological characteristics on it. However, the presence of oxide phases after laser modification could be determined by SIMS analysis with high accuracy. Laser-induced surface oxidation was reflected in the formation of ultra-thin oxide layers composed

from both Ti and Zr oxide phases. The sub-surface layers of least the first few layers (4–5 layers based on the SEM cross-section image) were intermixed and both oxide phases (Ti-oxide and Zr-oxide) existed on the contact surface, which was important for studying the cellular response. On the other hand, the pure oxygen signal was not registered in the spectrum, indicating that all the penetrated oxygen in the multilayer structure was in the form of compounds (oxides).

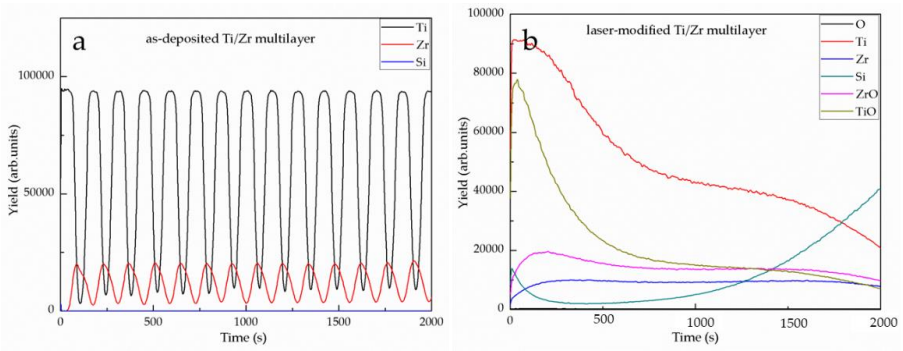

Figure 5. SIMS spectra before (**a**) and after (**b**) laser modification of 15×(Ti/Zr)/Si multilayer thin film.

Phase composition and crystal structure for as-deposited and laser-treated multilayer 30×(Ti/Zr)/Si system were determined by the XRD technique, as presented in Figure 6. All diffraction lines for Ti and Zr components were overlapped, because these elements were situated in the same group of periodic system one under another. In XRD pattern for as-deposited 30×(Ti/Zr)/Si multilayer system was identified both α-Ti and β-Ti phases (Figure 6a) at the following crystalline orientations α-Ti(100), β-Ti(110), α-Ti(102) and β-Ti(200) [28]. In this case, zirconium played a role as a β-stabiliser element, which induced the formation of β-Ti phases during the deposition of thin Ti and Zr layers [4]. Comparing the XRD patterns obtained for as-deposited and after laser processing of Ti/Zr multilayer thin film, it was observed that diffraction lines did not change positions. However, the intensities of these diffraction lines are changed, indicating that laser processing favored texture with dominant α-Ti(102) and β-Ti(200) crystalline orientation (Figure 6b).

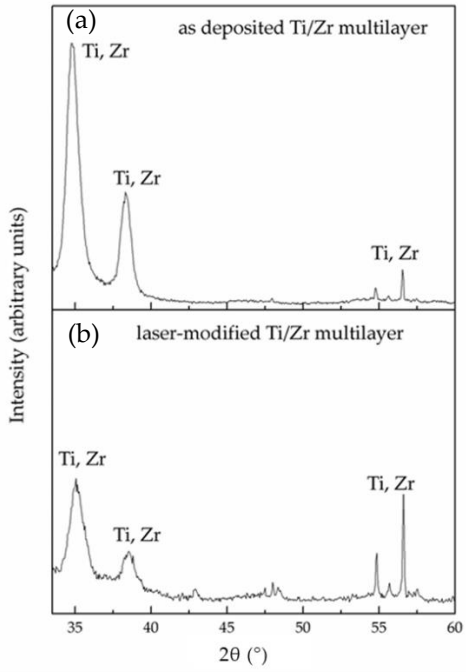

Figure 6. X-ray diffraction (XRD) patterns before (**a**) and after (**b**) laser modification of 15×(Ti/Zr)/Si multilayer thin film.

Before cell seeding on laser-processed 30×(Ti/Zr)/Si systems, the wettability was estimated by measuring the contact angle for as-deposited and laser-modified samples (Figure 7). In the experiment, estimation of the contact angle was determined the angle between the tangent of the solid surface and the tangent to the liquid (water) at the contact line among the three phases. The contact angle measurement included repeating the measurement five times, with an accuracy of 5%, for each surface just before seeding the cell culture. The contact angle for laser-modified Ti/Zr multilayer was greatly increased up to 136° value, which contributed to the achievement of a moderately hydrophobic surface. This increase in contact angle from the value of 82° for as-deposited sample was attributed to the formed surface topography in form of LIPSS with micro- and nanometer features, but also to the formation of Ti and Zr oxides on the contact surface [29]. Surface wettability can influence protein adsorption by controlling the total amount of proteins bound to the material, as well as their conformation and orientation after adsorption. The interaction between cells and Ti-based alloy can be considered through the dynamics of proteins when adsorbed onto the material surfaces. Proteins are structurally and chemically asymmetric, and during their adsorption the specific orientation and conformation were determined, defining the domain of the molecule that will interact and attach with the material [30].

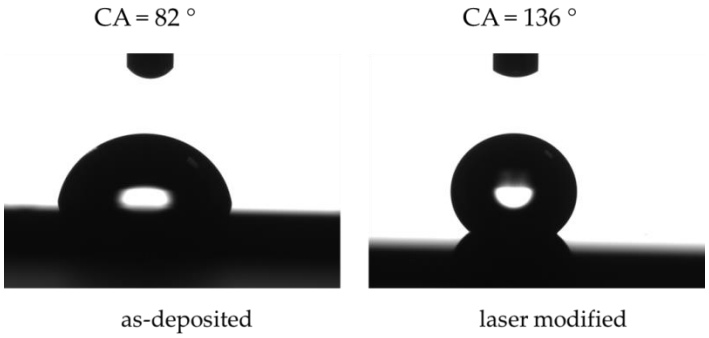

Figure 7. Contact angle measurements for as-deposited and laser modified surfaces of 30×(Ti/Zr) multilayer thin film.

The biocompatibility of the laser-modified Ti/Zr multilayers is reflected in cell adhesion and proliferation through contact, adhesion, and spreading in the initial phase of the cell-material interaction. Therefore, the laser-created surface topography with nano- and micro features plays a key role in further cellular behavior [31]. Morphological characteristics of MSCs cell proliferation on unmodified and laser-modified 30×(Ti/Zr)/Si multilayer surfaces was estimated by SEM and confocal analysis after one and three days' cultivation. After one-day cultivation on the surface of both unmodified and laser patterned Ti/Zr multilayers, the MSCs cells showed very good adhesion (Figure 8). On the as-deposited 30×(Ti/Zr)/Si sample with flat surfaces, there were easily visible cell groups an arbitrary cell growth occurring in all directions (Figure 8a,b), after one-day cultivation. On the other hand, under the same experimental conditions, on the 30×(Ti/Zr)/Si multilayer with laser-induced surface ripple morphology, the MSCs cells adhered, with a tendency for growth along the ripples' orientation (Figure 8c,d). In addition to the evident directed growth of osteoblast-like cells on a laser-created surface topography, it can be observed that the ripple morphology induced better communication between cells, due to significantly elongated cell groups with the aim to connect (Figure 8c,d). Statistically, a significantly larger number of cells per surface (250 μm × 250 μm) were attached on the laser-processed Ti/Zr multilayer (~80 cells) than to the flat as-deposited sample (~25 cells).

The proliferation of MSCs cells was achieved significantly, especially after three days when the number of cells was increased. Where almost whole surfaces were covered by cells for both as-deposited (flat surface) and laser-modified (ripple morphology) 30×(Ti/Zr)/Si samples after three-days cultivation (Figure 9). The number of cells for laser-modified 30×(Ti/Zr)/Si samples were about 220 cells per surface of 250 μm × 250 μm, while a slightly smaller number of cells about 170 cells were present on a

flat surface. Cell metabolic activities, determined by the MTT method including the measurement of the optical density at 545 nm, were found to result in approximately similar but statistically significant values (~42%) for both laser-modified and unmodified samples. It could be observed that the surface topography including micrometer sized laser-written lines with nanometer sized ripples did not influence on the cell proliferation rate. These facts can contribute to the conclusion that Ti/Zr multilayer systems have satisfactory biocompatibility regardless of surface conditions (Figure 9a,c). However, after three-day cultivation, the laser-modified surface was covered with a slightly larger number of smaller cells compared to as-deposited 30×(Ti/Zr)/Si multilayer, which was visible based on the cell cytoskeleton (Figure 9b,d). One of the most interesting findings is that osteoblast-like cells were oriented in all directions; they even had some kind of radial orientation in certain areas, in case of the as-deposited sample (Figure 9b). However, on the surface topography with ripples had a cell tendency to grow towards the ripples direction, with clear proliferation between one to three days (Figure 9d). Moreover, this study of the 30×(Ti/Zr)/Si multilayer demonstrated that in micro-line features, the ridge width is commonly larger than or equal to the size of a single cell, permissive for cell attachment and migration, as well as cell alignment following the geometrical guidance. In contrast, nano-ripple features are similar to the ECM (extracellular matrix) architectures and typically much smaller than a single cell, consequently inducing cell alignment in a more fundamental way such as mimicking or signaling the cell membrane receptors [32].

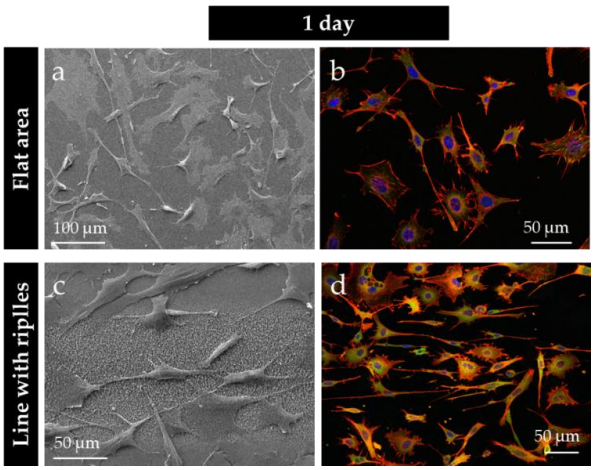

Figure 8. SEM and fluorescent images of mesenchymal stem cells (MSCs) osteoblast cultivated on the as-deposited (**a**,**b**), and laser-processed 30×(Ti/Zr)/Si multilayer thin film (**c**,**d**), for one-day cultivation, respectively.

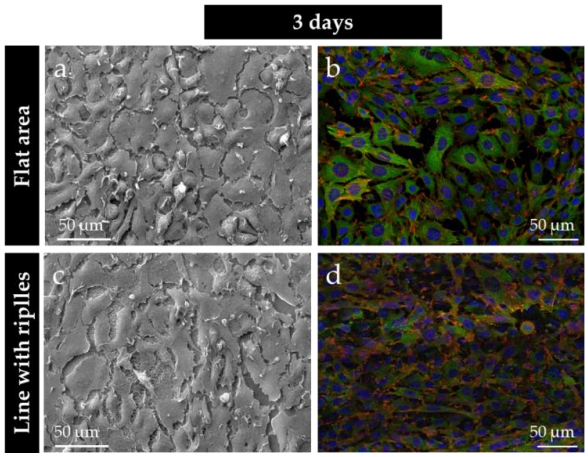

Figure 9. SEM and fluorescent images of MSCs osteoblast cultivated on the as-deposited (**a**,**b**), and laser-processed 30×(Ti/Zr)/Si multilayer thin film (**c**,**d**), for three-day cultivation, respectively.

4. Conclusions

The surface functionalization of the Ti-based alloy in terms of improving the osteoblast cell response was achieved by the deposition of a Ti/Zr multilayer structure and ultrafast laser processing. Adjusting the morphology and composition of the physical vapor-deposited 30×(Ti/Zr)/Si multilayer structure was achieved at optimal combination of laser parameters. The micro- and nanometer morphological features were obtained by laser writing micrometer sized lines on a relatively large 5 mm × 5 mm surface. In each laser-written line were created the laser-induced periodic surface structure defined as a low spatial frequency LIPSS (LSFL) with the periodicity close to 800 nm oriented normal to the laser polarization. While the space between the lines was filled with high spatial frequency LIPSS (HSFL) oriented perpendicular to LSFL ripples with periodicity of about 200 nm. The desired chemical composition required for good biocompatibility of Ti-based alloys was provided by the formation of a very thin oxide layer composed of Zr and Ti oxides, as well as intermixing of these components in the sub-surface region.

The biocompatibility of the laser-processed 30×(Ti/Zr)/Si multilayers was confirmed by the cultivation of a MSC-established adherent mouse osteoblast cell line. The osteoblast cells adhered and proliferated on the 30×(Ti/Zr)/Si multilayers, regardless of the fact that the samples were pre-laser treated to form specific surface topographies. However, after one- and three-day cultivation, the osteoblast cells showed a growth along ripples with a tendency to connection via their elongated parts, in the case of laser-patterned samples. Bioactivation of this specific 30×(Ti/Zr)/Si multilayer system with laser surface texturing and adjusting of surface composition could be potentially useful for tissue engineering and the application of this material as an implant.

Author Contributions: The contributions by author are as follows: conceptualization, S.P.; methodology, D.P., E.S. (Evangelos Skoulas), and Z.R.; formal analysis, J.K., M.M., J.P. and Z.R.; investigation, S.P. and D.P.; writing—original draft preparation, S.P.; writing—review and editing, S.P.; supervision, E.S. (Emmanuel Stratakis).

Funding: This research was funded by the EU-H2020 research and innovation program under grant agreement N 654360 having benefitted from the access provided by Foundation for Research and Technology Hellas (FORTH) access provider (Institute of Electronic Structure and Lasers i.e., Institution) in Heraklion, Crete, Greece within the framework of the NFFA-Europe Transnational Access Activity. This research was sponsored by the Ministry of Education, Science and Technological Development of the Republic Serbia through projects No. OI 171023, III 45016 and III45005.

Conflicts of Interest: The funders had no role in the design of the study; in the collection, analyses, or interpretation of data; in the writing of the manuscript, or in the decision to publish the results.

References

1. Othman, Z.; Cillero Pastor, B.; Van Rijt, S.; Habibovic, P. Understanding interactions between biomaterials and biological systems using proteomic. *Biomaterials* **2018**, *167*, 191–204. [CrossRef] [PubMed]
2. Su, Y.; Luo, C.; Zhang, Z.; Hermawan, H.; Zhu, D.; Huang, J.; Liang, Y.; Li, G.; Ren, L. Bioinspired surface functionalization of metallic biomaterials. *J. Mech. Behav. Biomed. Mater.* **2018**, *77*, 90–105. [CrossRef] [PubMed]
3. Bose, S.; Robertson, S.F.; Bandyopadhyay, A. Surface modification of biomaterials and biomedical devices using additive manufacturing. *Acta Biomater.* **2018**, *66*, 6–22. [CrossRef] [PubMed]
4. Correa, D.R.N.; Kuroda, P.A.B.; Lourenço, M.L.; Fernandes, C.J.C.; Buzalaf, M.A.R.; Zambuzzi, W.F.; Grandini, C.R. Development of Ti-15Zr-Mo alloys for applying as implantable biomedical devices. *J. Alloy. Compd.* **2018**, *749*, 163–171. [CrossRef]
5. Rack, H.J.; Qazi, J.I. Titanium alloys for biomedical applications. *Mater. Sci. Eng. C* **2006**, *26*, 1269–1277. [CrossRef]
6. Donato, T.A.G.; De Almeida, L.H.; Nogueira, R.A.; Niemeyer, T.C.; Grandini, C.R.; Caram, R.; Schneider, S.G.; Santos, A.R., Jr. Cytotoxicity study of some Ti alloys used as biomaterial. *Mater. Sci. Eng. C* **2009**, *29*, 1365–1369. [CrossRef]
7. Zhao, D.; Chen, C.; Yao, K.; Shi, X.; Wang, Z.; Hahn, H.; Gleiter, H.; Chen, N. Designing biocompatible Ti-based amorphous thin films with no toxic element. *J. Alloy. Compd.* **2017**, *707*, 142–147. [CrossRef]

8. Hsu, H.C.; Wu, S.C.; Sung, Y.C.; Ho, W.F. The structure and mechanical properties of as-cast Zr-Ti alloys. *J. Alloy. Compd.* **2009**, *488*, 279–283. [CrossRef]
9. Li, Y.; Yang, C.; Zhao, H.; Qu, S.; Li, X.; Li, Y. New developments of Ti-based alloys for biomedical applications. *Materials* **2014**, *7*, 1709–1800. [CrossRef]
10. Aristizabala, M.; Jamshidib, P.; Sabooric, A.; Coxd, S.C.; Attallah, M.M. Laser powder bed fusion of a Zr-alloy: Tensile properties and biocompatibility. *Mater. Lett.* **2020**, *259*, 126897. [CrossRef]
11. Yu, Z.; Yang, G.; Zhang, W.; Hu, J. Investigating the effect of picosecond laser texturing on microstructure and biofunctionalization of titanium alloy. *J. Mater. Process. Tech.* **2018**, *255*, 129–136. [CrossRef]
12. Sartinska, L.L.; Barchikovski, B.; Wagenda, N.; Rut, B.M.; Timofeeva, I.I. Laser induced modification of surface structures. *Appl. Surf. Sci.* **2007**, *253*, 4296–4299. [CrossRef]
13. Frostevarg, J.; Olsson, R.; Powell, J.; Palmquist, A.; Branemark, R. Formation mechanisms of surfaces for osseointegration on titanium using pulsed laser spattering. *Appl. Surf. Sci.* **2019**, *485*, 158–169. [CrossRef]
14. Berg, Y.; Kotler, Z.; Shacham-Diamand, Y. Holes generation in glass using large spot femtosecond laser pulses. *J. Micromech. Microeng.* **2018**, *28*, 035009. [CrossRef]
15. Jenko, M.; Gorensek, M.; Godec, M.; Hodnik, M.; Setina-Batic, B.; Donik, C.; Grant, J.T.; Dolinar, D. Surface chemistry and microstructure of metallic biomaterials for hip and knee endoprostheses. *Appl. Surf. Sci.* **2018**, *427*, 584–593. [CrossRef]
16. Simitzi, C.; Ranella, A.; Stratakis, E. Controlling the morphology and outgrowth of nerve and neuroglial cells: The effect of surface topography. *Acta Biomater.* **2017**, *51*, 21–52. [CrossRef]
17. Gregorcic, P.; Sedlacek, M.; Podgornik, B.; Reif, J. Formation of laser-induced periodic surface structures (LIPSS) on tool steel by multiple picosecond laser pulses of different polarizations. *Appl. Surf. Sci.* **2016**, *387*, 698–706. [CrossRef]
18. Varlamova, O.; Costache, F.; Reif, J.; Bestehorn, M. Self-organized pattern formation upon femtosecond laser ablation by circularly polarized light. *Appl. Surf. Sci.* **2006**, *252*, 4702–4706. [CrossRef]
19. Gittens, R.A.; Lachlan, T.M.; Olivares-Navarrete, R.; Cai, Y.; Berner, S.; Tannenbaum, R.; Schwartz, Z.; Sandhage, K.H.; Boyan, B.D. The effects of combined micron-/submicron-scale surface roughness and nanoscale features on cell proliferation and differentiation. *Biomaterials* **2011**, *32*, 3395–3403. [CrossRef]
20. Stanciuc, A.M.; Flamant, Q.; Sprecher, C.M.; Alini, M.; Anglada, M.; Peroglio, M. Femtosecond laser multi-patterning of zirconia for screening of cell-surface interactions. *J. Eur. Ceram. Soc.* **2018**, *38*, 939–948. [CrossRef]
21. Ohtsu, N.; Kozuka, T.; Yamane, M.; Arai, H. Surface chemistry and osteoblast-like cell response on a titanium surface modified by a focused Nd: YAG laser. *Surf. Coat. Technol.* **2017**, *309*, 220–226. [CrossRef]
22. Bonse, J.; Koter, R.; Hartelt, M.; Spaltmann, D.; Pentzien, S.; Hohm, S.; Rosenfeld, A.; Krüger, J. Tribological performance of femtosecond laser-induced periodic surface structures on titanium and a high toughness bearing steel. *Appl. Surf. Sci.* **2015**, *336*, 21–27. [CrossRef]
23. Kirnera, S.V.; Wirth, T.; Sturm, H.; Krüger, J.; Bonse, J. Nanometer-resolved chemical analyses of femtosecond laser-induced periodic surface structures on titanium. *J. Appl. Phys.* **2017**, *122*, 104901. [CrossRef]
24. Može, M.; Zupančič, M.; Hočevar, M.; Golobič, I.; Gregorčič, P. Surface chemistry and morphology transition induced by critical heat flux incipience on laser-textured copper surfaces. *Appl. Surf. Sci.* **2019**, *490*, 220–230. [CrossRef]
25. Petrović, S.; Peruško, D.; Kovač, J.; Panjan, P.; Mitrić, M.; Pjević, D.; Kovačević, A.; Jelenković, B. Design of co-existence parallel periodic surface structure induced by picosecond laser pulses on the Al/Ti multilayers. *J. Appl. Phys.* **2017**, *122*, 115302. [CrossRef]
26. Oh, H.; Pyatenko, A.; Lee, M. Laser dewetting behaviors of Ag and Au thin films on glass and Si substrates: Experiments and theoretical considerations. *Appl. Surf. Sci.* **2019**, *475*, 740–747. [CrossRef]
27. Abbott, W.M.; Corbett, S.; Cunningham, G.; Petford-Long, A.; Zhang, S.; Donegan, J.F.; McCloskey, D. Solid state dewetting of thin plasmonic films under focused cw-laser irradiation. *Acta Mater.* **2018**, *145*, 210–219. [CrossRef]
28. JCPDS. *International Centre for Diffraction Data (ICDD), PCPDFWIN v. 2.00*; ICDD: Newtown Square, PA, USA, 1998.
29. Bizi-Bandoki, P.; Benayoun, S.; Valette, S.; Beaugiraud, B.; Audouard, E. Modifications of roughness and wettability properties of metals induced by femtosecond laser treatment. *Appl. Surf. Sci.* **2011**, *257*, 5213–5218. [CrossRef]

30. Tang, L.; Thevenot, P.; Hu, W. Surface chemistry influence implant biocompatibility. *Curr. Top. Med. Chem.* **2008**, *8*, 270–280. [CrossRef]
31. Anselme, K. Osteoblast adhesion on biomaterials. *Biomaterials* **2000**, *21*, 667–681. [CrossRef]
32. Babaliari, E.; Kavatzikidou, P.; Angelaki, D.; Chaniotaki, L.; Manousaki, A.; Siakouli-Galanopoulou, A.; Ranella, A.; Stratakis, E. Engineering Cell Adhesion and Orientation via Ultrafast Laser Fabricated Microstructured Substrates. *Int. J. Mol. Sci.* **2018**, *19*, 2053. [CrossRef] [PubMed]